

# Reversible Gel Formation of Triblock Copolymers Studied by Molecular Dynamics Simulation

Lei Guo and Erik Luijten\*

*Department of Materials Science and Engineering,*

*University of Illinois at Urbana-Champaign, 1304 West Green Street, Urbana, Illinois 61801*

(Dated: September 1, 2004; revised version October 12, 2004)

Molecular dynamics simulations have been employed to study the formation of a physical (thermoreversible) gel by amphiphilic A-B-A triblock copolymers in aqueous solution. In order to mimic the structure of hydrogel-forming polypeptides employed in experiments [W.A. Petka *et al.*, *Science* **281**, 389 (1998)], the endblocks of the polymer chains are modeled as hydrophobic rods representing the alpha-helical part of the polypeptides whereas the central B-block is hydrophilic and semi-flexible. We have determined structural properties, such as the hydrophobic cluster-size distribution function, the geometric percolation point and pair correlation functions, and related these to the dynamical properties of the system. Upon decrease of the temperature, a network structure is formed in which bundles of endblocks act as network junctions. Both at short and medium distances an increased ordering is observed, as characterized by the pair correlation function. Micelle formation and the corresponding onset of geometric percolation induce a strong change in dynamical quantities, e.g., in the diffusion constant and the viscosity, and causes the system to deviate from the Stokes–Einstein relation. The dynamical properties show a temperature dependence that is strongly reminiscent of the behavior of glass-forming liquids. The appearance of a plateau in the stress autocorrelation function suggests that the system starts to exhibit a solid-like response to applied stress once the network structure has been formed, although the actual sol–gel transition occurs only at a considerably lower temperature.

Keywords: molecular dynamics simulation, triblock copolymers, sol–gel transition, percolation transition

## I. INTRODUCTION

Solutions of polymers with attractive groups (associating polymers) exhibit a wide range of rheological properties that can be controlled through variation of temperature and concentration. These materials enjoy applications ranging from viscosity modifiers in food or oil recovery to adhesives and coatings (see Ref. [1] and references therein). Under certain conditions, the attractive groups of the polymers associate to form a network and the system undergoes a sol–gel transition. The physical bonds between the attractive groups are reversible and, depending on their strength, can break and reform frequently on experimental time scales. The properties of these so-called *weak* or physical gels differ markedly from chemical gels in which the polymers are interconnected through covalent bonds. Compared to chemical gels, the current understanding of physical gelation is still limited and even controversial [1]. Scenarios for thermoreversible gelation include the possibility of *discontinuous* gelation, in which the gelation is accompanied by sol–gel phase separation, and *continuous* gelation. The theoretical treatments of Tanaka and Stockmayer [2, 3, 4, 5] predict that continuous gelation is a thermodynamic phase transition, whereas Semenov and Rubinstein arrive at the opposite conclusion [6].

Simulations can provide specific information that is not easily obtained otherwise. On the one hand, the mi-

croscopic structure of physical gels is difficult to determine experimentally, whereas it can be directly accessed (within the limitations of the model used) by means of simulations. On the other hand, the numerical calculations permit testing of theoretical hypotheses and approximations. Two models are widely used to study associating polymers. In the first category of models, used in the above-mentioned theories, there are many association sites (“stickers”) distributed along the polymer chain. This model was studied extensively in early (off-lattice) Monte Carlo simulations by Groot and Agterof [7, 8, 9]. Kumar and Panagiotopoulos [10] have investigated the thermodynamic properties of a lattice-based version of this model by Monte Carlo simulations and did not find any indication that gelation is a thermodynamic phase transition. More recently, it has been observed that the dynamical properties of this model are similar to those of weak glass formers, in which the diffusion coefficient is described by an expression with a Vogel–Fulcher form [11].

The second category of models consists of *telechelic* chains, in which the associative sites are located at both chain ends and typically represented by a single monomer (see Ref. [12] for a concise overview). At low concentrations, these chains have been predicted to form flower-like micelles [13]. Simulations have indeed confirmed this [14, 15] and found that the associative groups are located in the core of the micelles and the non-associative groups in the corona. At higher concentrations, micelles can be connected by “bridging” polymers for which both associative endgroups belong to different micelles, leading to the formation of a micellar gel. The dynamics in such a system are governed by the hopping rate of the

---

\*Corresponding author; e-mail: luijten@uiuc.edu

associative groups between different micelles [13]. Simulations have indeed found that the diffusion properties of such solutions can be described by an Arrhenius law [15], as predicted by Tanaka and Edwards [16]. If the polymer chains are less flexible, qualitative structural changes occur, as intra-chain pairing is suppressed and the formation of flower-like micelles becomes energetically unfavorable. This promotes the formation of a network structure at low polymer concentrations [17]. However, the dynamical properties of such solutions of semiflexible telechelic chains seem not to have been investigated.

Recently, Petka *et al.* [18] have used genetic engineering techniques to create artificial proteins consisting of a hydrophilic group flanked by two stiff hydrophobic blocks. This triblock copolymer was found to exhibit gelation in response to variation of pH or temperature. Its significance lies in the possibility to independently tune the strength of the endgroup attractions that are responsible for gelation and the solvent retention capability of the chains, which is essential for the formation of a swollen gel. However, the actual structure of the hydrogel, which is formed at low polymer concentrations, could only be conjectured. Motivated by the experimental findings, we have employed molecular dynamics simulations to investigate the dynamic and structural properties of a solution of triblock copolymers that can be viewed as a greatly simplified, coarse-grained model of the artificial proteins. This model evidently does not capture all relevant properties of the experimental systems, but rather should be viewed as a first attempt to determine the generic properties of a solution of triblock copolymers with two stiff endgroups.

## II. MODEL AND SIMULATIONAL DETAILS

In order to study the gelation of triblock copolymers we employ molecular dynamics simulations, using the DL-POLY\_2 code [19]. The polymers have an A-B-A structure, where the A-blocks are rigid hydrophobic rods and the B-block is hydrophilic and semiflexible. In our coarse-grained model, the solvent is modeled implicitly and each copolymer block is composed of spherical units (“monomers”) that represent an effective segment. The total length of each chain is set to 15 units, consisting of three A-monomers per hydrophobic block and nine B-monomers in the hydrophilic block. This choice is mostly based upon practical considerations. A minimum of three units is required to represent a rod-like endblock, whereas a longer central block would pose equilibration problems, given the computationally accessible time scales. Monomers of type A interact via an attractive Lennard-Jones potential,

$$U_{AA} = 4\varepsilon_{AA} \left[ \left( \frac{\sigma_{AA}}{r} \right)^{12} - \left( \frac{\sigma_{AA}}{r} \right)^6 \right], \quad (1)$$

whereas the interactions between monomers of type B and the interactions between unlike pairs are purely re-

pulsive,

$$\begin{aligned} U_{BB} &= 4\varepsilon_{BB} \left( \frac{\sigma_{BB}}{r} \right)^{12} \\ U_{AB} &= 4\varepsilon_{AB} \left( \frac{\sigma_{AB}}{r} \right)^{12}. \end{aligned} \quad (2)$$

We set  $\varepsilon_{AA} = \varepsilon_{BB} = \varepsilon_{AB} = \varepsilon$  and  $\sigma_{AA} = \sigma_{BB} = \sigma_{AB} = \sigma$  and cut off all interactions at  $2.5\sigma$ . In order to express our results in reduced units we use  $\varepsilon$  and  $\sigma$  as units of energy and length, respectively. The reduced coupling, or inverse reduced temperature,  $J \equiv \varepsilon/k_B T$  is varied between 1 and 2 in the simulations. The semiflexible character of the hydrophilic block is controlled by a harmonic angle-dependent potential,

$$U_\theta = \frac{1}{2}k_\theta(\theta - \theta_0)^2, \quad (3)$$

where  $k_\theta = 10\varepsilon/\text{degree}^2$  and  $\theta_0 = 175^\circ$ . The value of  $\theta_0$  was chosen in accordance with the model proposed in Ref. [17]. In combination with the large value for  $k_\theta$  it causes the chains to adopt an extended structure (but without having the rod-like structure that would be obtained for  $\theta_0 = 180^\circ$ ), and gelation is anticipated to occur at relatively low polymer concentrations. The  $\alpha$ -helical structure in the artificial proteins [18] is mimicked by making the endblocks fully rigid. All monomer units within a chain are connected via a harmonic bond potential

$$U_{\text{bond}} = \frac{1}{2}k_{\text{bond}}(r - r_0)^2, \quad (4)$$

where  $k_{\text{bond}} = 170\varepsilon/\sigma^2$  and  $r_0 = 1.30\sigma$ .

The simulations are performed in the canonical ( $NVT$ ) ensemble, in a cubic box of linear dimension  $L = 39\sigma$  with periodic boundary conditions. The total number of chains equals  $N = 216$ , corresponding to a monomeric packing fraction of only 0.029, i.e., roughly twice the overlap threshold. The temperature is controlled by means of the Nosé-Hoover thermostat [20]. The equations of motion are integrated using a “leap-frog” Verlet scheme [21], with a time step (in reduced units)  $\Delta t = 0.00287$ . In all runs, the system is first equilibrated for four million steps; for some low temperatures, even longer equilibration periods are used. Subsequently, 40 million time steps are carried out for high temperatures and 200 million time steps for low temperatures. After the equilibration period, the configuration of the system is recorded every 1000 time steps for analysis of structural (e.g., chain conformations and percolation of the system) and dynamical (e.g., single-chain diffusion) properties. In addition, the energies and the stress tensors are calculated and recorded every 100 time steps for the calculation of the specific heat and the stress autocorrelation function.

Despite the simplifications made in this coarse-grained model, the required simulation effort is still appreciable. The total amount of CPU time corresponds to approximately 2.5 years on a single 2.0GHz Intel Xeon processor.

### III. SIMULATION RESULTS

#### A. Structural properties

In order to characterize structural changes that take place in this system upon variation of the temperature, we employ an approach used in the study of micelle formation. For each configuration, bundles of endblocks are identified. An endblock is considered part of a bundle if its center monomer lies within a distance  $r_c$  from the center monomer of an endblock that is already part of the bundle. Our results turn out to be insensitive to the precise value of  $r_c \in [\sigma, 4\sigma]$  and we have chosen  $r_c = 2\sigma$ . A configuration contains  $N(m)$  bundles of  $m$  endblocks and the bundle-size distribution is defined as the thermal average [17]

$$W(m) = \frac{\langle N(m) \rangle}{\langle \sum_m N(m) \rangle}. \quad (5)$$

Figure 1 shows  $W(m)$  for five values of the inverse temperature  $J$ , illustrating the formation of bundles of hydrophobic blocks as the temperature is lowered. At high temperature ( $J = 1.00$ ), the distribution function decays monotonically, with a single peak at  $m = 1$  (isolated endblocks). This corresponds to a regular solution of chains that are not associated. For lower temperatures ( $J > 1.15$ ), however, an additional “shoulder” appears in the distribution function, which develops into a peak that increases in height and shifts to larger bundle sizes if the temperature is further decreased. This signals the formation of bundles in which large numbers of hydrophobic endblocks participate, resulting in important structural changes in the solution. The occurrence of an inflection point in  $W(m)$  has been taken as a criterion for the critical micelle point [17]. Here, we associate the appearance of a shoulder in Fig. 1 with the onset of the bundling process. The corresponding characteristic inverse temperature  $J^*$  lies between 1.15 and 1.20.

A similar criterion was employed in Ref. [15] [but note that the quantity  $P(m)$  employed in this reference differs from  $W(m)$ ], and a comparable temperature dependence was observed for the bundle-size distribution. There is, however, a marked difference in the morphology of the bundles. The flexible telechelic polymers studied in Ref. [15] form flower-like micelles in which the chains take the shape of a loop. Both endgroups of each chain lie in the core of the same micelle and the central block lies in the corona [17]. For more rigid chains, two effects occur. The stiff endblocks have a tendency to align inside the bundle, giving it the appearance of a microcrystalline domain. In addition, the semiflexible character of the central block prevents the chain from adopting a loop-like conformation. This second effect is illustrated in Fig. 2, in which we compare the average number of endblocks per bundle to the average number of endblocks in a bundle that belong to the same chain. As shown, single-chain loops are essentially absent at all temperatures, confirm-

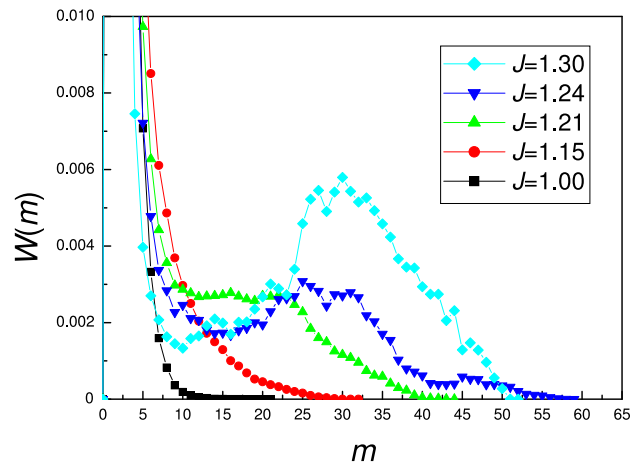


FIG. 1: Bundle-size distribution [probability  $W(m)$  of encountering a bundle containing  $m$  endblocks] for five representative values of the inverse temperature  $J$ . The appearance of a secondary peak characterizes the formation of bundles in the solution.

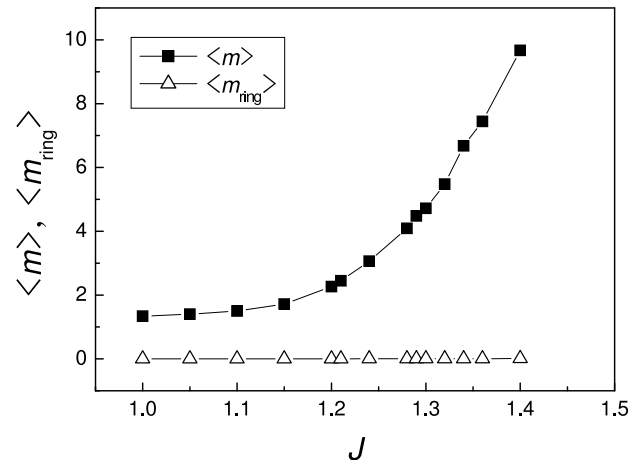


FIG. 2: Comparison between the average number of endblocks per bundle (closed squares) and the average number of endblocks per bundle that form a loop-like structure (open triangles). Whereas the average bundle size increases upon increasing coupling  $J$  (decreasing temperature), the average number of loops remains negligibly small. The rigidity of the chains thus prevents the formation of “flower-like” micelles in the solution. Error bars are smaller than the symbol size.

ing the prohibitively large energy penalty incurred by ring formation.

Instead, each chain takes an extended conformation, with both hydrophobic endgroups participating in different bundles. Thus, even the formation of a continuous network becomes possible, in which the bundles of endblocks act as network junction points [17]. However, following the experimental observations in Ref. [18], we have chosen a markedly lower concentration than in earlier simulation studies. Before investigating whether the formation of a network is nevertheless possible, we consider the energetic aspects of bundling. As illustrated

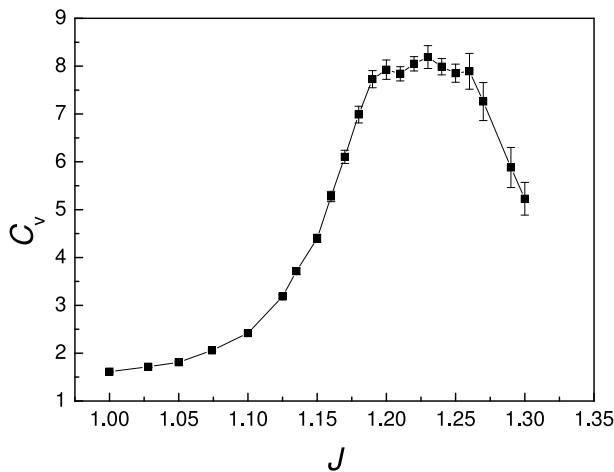


FIG. 3: The specific heat  $C_V$  (in reduced units) as a function of inverse temperature  $J$ . The maximum is indicative of bundle formation in the system. The line serves as a guide to the eye.

in Fig. 3, the specific heat  $C_V$  exhibits a pronounced but relatively broad maximum around  $J = 1.23$ , corresponding to the creation of bundles of attractive endblocks. The specific-heat maximum was found to occur at a temperature *below* the onset of micelle formation (at  $J = J^*$ ) in Ref. [15]. Our data do not permit us to conclude this unambiguously. Indeed, for  $J \gtrsim 1.20$  the simulations become almost prohibitively expensive, owing to the slow dynamic evolution of the system. Thus, the present system does not lend itself well to the application of finite-size scaling techniques for the determination of the nature and precise location of the bundling transition. For example, in case of a continuous phase transition, the height of the specific-heat maximum will increase (up to corrections to scaling) as  $L^{\alpha/\nu} \propto N^{\alpha/(3\nu)}$ . The exponent  $\alpha/(3\nu)$  is typically rather small (e.g., 0.058 for Ising-type criticality [22]), so that even doubling the number of chains would only increase the peak height by an amount comparable to the statistical accuracy of the data.

In order to determine whether bundle formation indeed leads to the emergence of a connected network structure, we consider the percolation probability. Geometric percolation of the polymer chains in the solution is a necessary condition for gelation. However, whereas *chemical* gelation coincides with the occurrence of geometric percolation [23], *physical* gelation has been suggested to take place only far below the percolation point [11]. We consider our polymer solution to be percolating if a connected path (composed of chains that bridge the bundles of endblocks) exists between any pair of opposite sides of the simulation cell. The percolation probability, which is defined as the probability that a configuration is percolating, is plotted as a function of inverse temperature in Fig. 4. The system always percolates for  $J \gtrsim 1.15$ , i.e., near the characteristic inverse temperature  $J^*$  for bundle formation. As the percolation probability certainly can

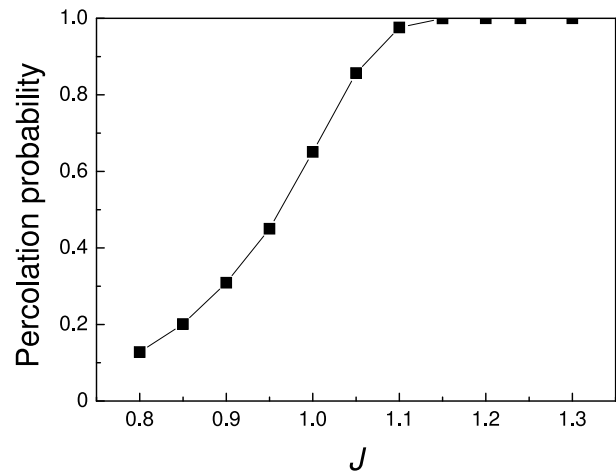


FIG. 4: Percolation probability of a solution of associative telechelic polymers at a monomeric packing fraction  $\phi = 0.029$ , as a function of inverse temperature  $J$ . Since the percolation probability equals unity for  $J \gtrsim 1.15$ , we consider this to be a measure for the percolation threshold.

exhibit strong finite-size effects, this determination must only be viewed as an estimate for the percolation threshold in the thermodynamic limit. The observation that  $J^*$  and the percolation threshold coincide reaffirms our interpretation that the telechelic chains become interconnected through bundle formation and form an spanning network. This behavior appears to differ from what has been observed for the solution of flexible telechelic chains studied in Ref. [15], which exhibits a comparable temperature dependence in the bundle-size distribution but is reported to exhibit geometric percolation at all temperatures. Figure 5 shows a typical configuration, obtained in a simulation performed at  $J = 1.30$ . A network of interconnected hydrophobic junction points is indeed clearly discernable.

The onset of percolation affects the single-chain conformations as well. This is illustrated by means of the temperature dependence of the end-to-end distance  $R_e$ , see Fig. 6. For comparison, the figure also includes the end-to-end distance for an identical system in which the monomers in the endblocks experience a purely repulsive interaction [see Eq. (2)]. Whereas  $R_e$  increases for both systems as the temperature is lowered, the end-to-end distance increases more rapidly for the chains with attractive endblocks than for the purely repulsive chains. Because of the semiflexible character of the chains, the *relative* change in  $R_e$  is only several percent, but nevertheless the effect is clearly most pronounced for  $J \gtrsim 1.15$ , i.e., near the percolation threshold  $J^*$ . We ascribe it to the conformational changes induced by the network formation. Owing to the low polymer concentration, the bundles are relatively widely separated, forcing the connecting chains to adopt an extended conformation. This observation is reinforced by considering the spatial correlations between endblocks.

Indeed, the rod-like structure of the hydrophobic end-

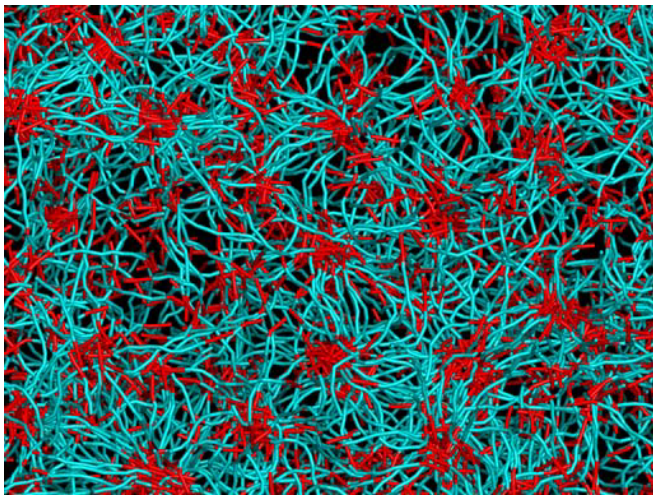


FIG. 5: Snapshot of a simulation at  $J = 1.30$ , for a system of linear size  $L = 78\sigma$  (monomer packing fraction 0.029). The image represents approximately two-thirds of the simulation box. The hydrophobic endblocks are shown in red and the hydrophilic groups in cyan. The extended structure of individual chains as well as the bundling of hydrophobic blocks (cf. the peak in Fig. 1) can clearly be seen.

blocks leads to an internal structure in the bundles that is absent in the models studied in Refs. [15, 17]. Figure 7 shows the hydrophobe–hydrophobe radial distribution function  $g(r)$  (calculated from their center-of-mass separation) at different values of  $J$ . As the temperature is decreased, two distinct features can be identified in this distribution function. The increasing maxima at short separations, which all lie at distances within the bundle size (cf. Fig. 1), correspond to intra-bundle alignment of endblocks. The emergence of this microcrystalline morphology can be understood from the fact that in an aligned bundle each endblock experiences a large number of monomer–monomer interactions with surrounding endblocks. The cutoff distance employed in the Lennard-Jones potential (1) is larger than the maximum distance between monomers on fully-aligned (close-packed) endblocks, so that even a single pair of rods can have 9 pair interactions. As shown in Fig. 2, the average number of rods per bundle increases rapidly from approximately 2 at  $J = 1.15$  to almost 10 at  $J = 1.40$ , leading to tightly-bonded bundles. It is this bonding that makes the resulting network resistant to external stress. A second feature arises in Fig. 7 at lower temperatures. As shown in the inset, an additional peak appears at a position that roughly coincides with the calculated average bundle separation, which varies from 13 at  $J = 1.15$  to 15 at  $J = 1.30$ . Thus, this peak characterizes the ordered arrangement of the bundles at low temperatures, and we conclude that the radial distribution function reflects the simultaneous emergence of both short-range and medium-range order upon cooling.

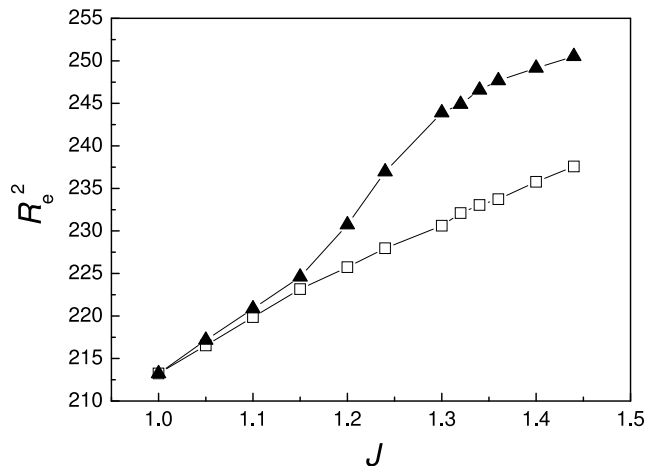


FIG. 6: Square of the end-to-end distance  $R_e$  of the telechelic chains (closed triangles), as a function of inverse temperature  $J$ . For comparison, this graph also shows the end-to-end distance for identical chains in which the endblocks do *not* possess an attractive interaction (open squares). For both chain types,  $R_e$  increases upon increasing  $J$  (decreasing temperature), reflecting the decreasing flexibility of the center blocks. However, for  $J > J^* \approx 1.15$  the telechelic chains clearly exhibit a stronger tendency to adopt an extended structure, which is attributed to the formation of an interconnected network. Error bars are smaller than the symbol size.

## B. Dynamical properties

In order to determine whether the structural changes observed in the triblock copolymer solution indeed correspond to gelation, we consider the dynamical properties as a function of temperature. Evidently, bundle formation and the formation of a percolating network are anticipated to have a strong influence on the diffusion properties of the polymers. Figure 8 shows the mean-square displacement of the center-of-mass of polymers at different values for  $J$ . At high temperatures, we observe the standard behavior in which the dynamics cross over from ballistic motion at short times to diffusive motion at long times. At low temperatures, an intermediate regime appears where the dynamics are slowed down, indicative of the arrested dynamics resulting from network formation. Comparable observations were reported by Kumar and Douglas [11] in a Monte Carlo study of a lattice model of an associating polymer solution and by Bedrov *et al.* [15] for micellar solutions, although it should be noted that in both studies the polymer concentration was considerably higher than in the current system (which has  $c/c^* \approx 2$ ) and that in the micellar system the change in dynamic behavior was not associated with the formation of a network structure. The dynamic behavior seen in the low-density gel is similar to that found in glass-forming materials, but the underlying mechanism is different. The temporary localization of the triblock copolymers is caused by the strong intra-bundle interactions experienced by the

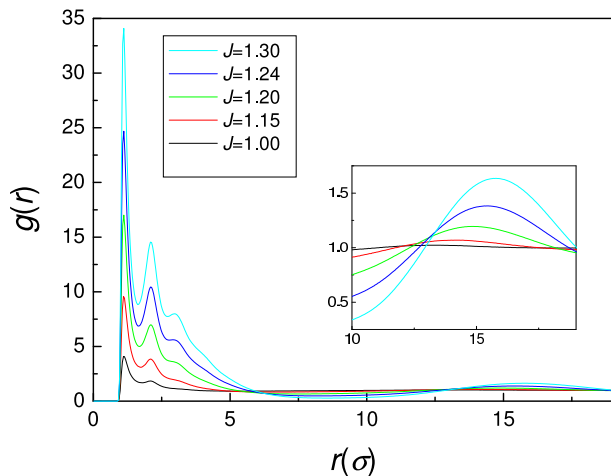


FIG. 7: Hydrophobe-hydrophobe radial distribution function at different values of the inverse temperature  $J$ . At short distances, the existing peaks increase and new peaks emerge as  $J$  increases, an indication of the alignment of the rigid hydrophobic rods within a bundle toward a microcrystalline-like structure. At long distances, a new peak appears at the average bundle-to-bundle distance and grows higher at higher  $J$ , suggesting the structured arrangement of the bundles.

endblocks, rather than by caging or jamming effects. We also note that the width of the ballistic regime depends on the simulation model. If water molecules are included explicitly or implicitly via a friction coefficient (Brownian dynamics), the ballistic regime may be rather narrow or even not observable at all. For all investigated temperatures, the polymers eventually diffuse and we extract the diffusion coefficient  $D$  from this long-time behavior, see Fig. 9. At low temperatures, a second (narrow) diffusive regime arises for times between the ballistic and the intermediate regime. This corresponds to intra-domain motion of the endblocks.

The diffusion coefficient exhibits an exponential dependence on inverse temperature over the entire temperature range that we investigated, but two regimes can be discerned, separated near  $J^* \approx 1.15$ . Since both percolation and micelle formation occur near this temperature, it is not possible to uniquely attribute the strong decrease of  $D$  to either of these two phenomena. For the “sticker” model of Ref. [11], in which association sites are distributed along the polymer chain, the diffusion coefficient was found to be well described by a Vogel-Fulcher law. In our system, the diffusive dynamics follow an Arrhenius law,  $D \propto \exp(-E/k_B T)$ , where  $E$  is the effective activation energy, similar to strong glass-formers (cf. Ref. [24]) and micelle-forming telechelic polymers [15]. The Arrhenius-type behavior suggests that dynamic relaxation, which takes place through the exchange of an endblock between two bundles (network junctions), is controlled by an energetic barrier. This barrier has a clear thermodynamic origin, namely the strong attraction between endblocks. From Fig. 9,  $E$  is estimated to be approximately  $10\varepsilon$  in the low-temperature regime,

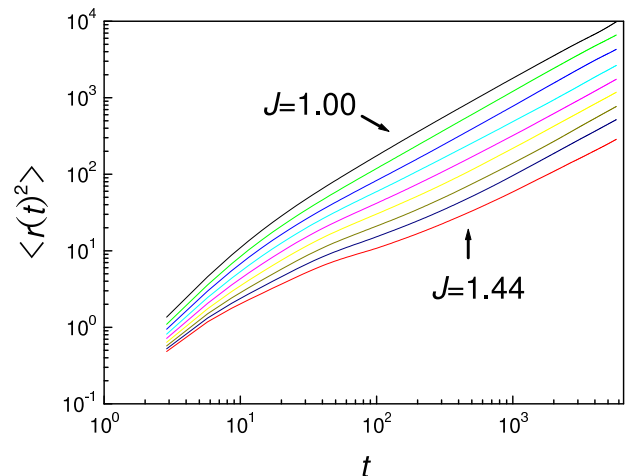


FIG. 8: Mean-square displacement  $\langle r(t)^2 \rangle$  of the single-chain center-of-mass, for inverse temperatures  $J = 1.00, 1.15, 1.20, 1.24, 1.28, 1.32, 1.36, 1.40, 1.44$  (only the lowest and highest value for  $J$  are labeled). In addition to ballistic motion at short times and diffusive motion at long times, a slow intermediate regime appears at low temperatures.

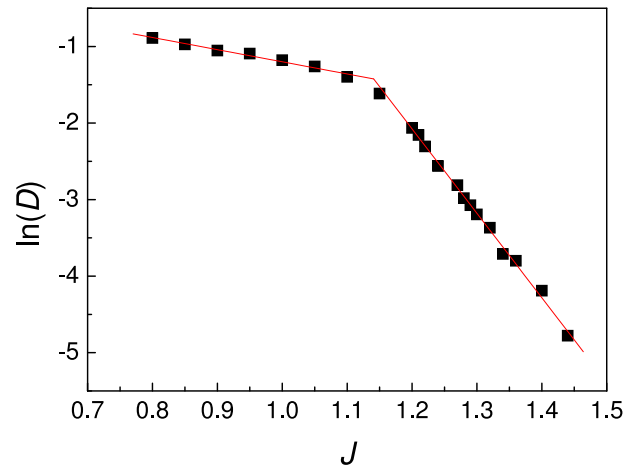


FIG. 9: Diffusion coefficient  $D$  as a function of inverse temperature  $J$  on a log-linear scale. There are two regimes with a different exponential dependence on  $J$ , which are joined near the percolation point  $J^* \approx 1.15$ . While the high-temperature data ( $J < J^*$ ) only permit an approximate fit, the diffusion coefficient in the low-temperature regime is clearly well described by an Arrhenius law, suggesting that activated processes control the relaxation of the system. Error bars are of the order of the symbol size or less.

consistent with our earlier estimate of the number of interacting monomers in a pair of hydrophobic rods. Interestingly, the similarity between the dynamic properties observed in this system and those of the micellar system studied in Ref. [15] suggest that while the semiflexible character of the center blocks and the presence of rod-like hydrophobic endblocks change the structural properties of the solution, these differences do not qualitatively affect the dynamic behavior.

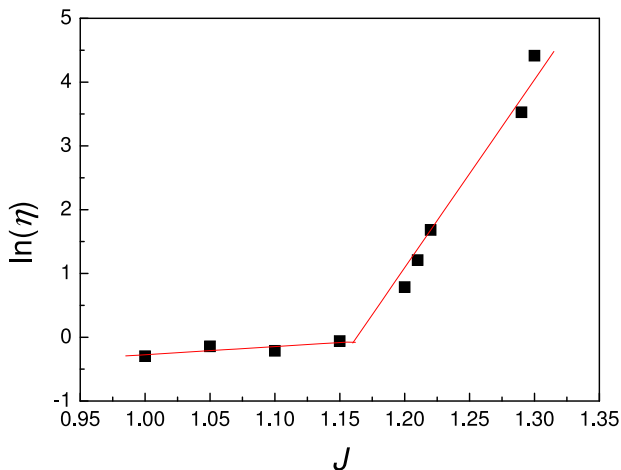


FIG. 10: The viscosity  $\eta$  at different couplings on a log-linear scale. Similar to  $D$ ,  $\eta$  behaves differently in two regions divided at the percolation point  $J^* = 1.15$ . In both regions  $\eta$  can be well described by an Arrhenius law. Scatter in the data at low temperatures is caused by uncertainties in the numerical integration (6).

Since gelation will be accompanied by a dramatic increase in viscosity  $\eta$ , we compute this quantity by integrating the stress autocorrelation function  $G(t)$  [25],

$$\eta = \int_0^{+\infty} G(t) dt. \quad (6)$$

Here,  $G(t)$  is defined as

$$G(t) = \frac{V}{3k_B T} \sum_{\alpha\beta} \langle \sigma_{\alpha\beta}(t_0) \sigma_{\alpha\beta}(t_0 + t) \rangle, \quad (7)$$

where  $V$  is the volume of the system and  $\alpha\beta$  assumes the values  $xy, yz, zx$ . The average  $\langle \dots \rangle$  is taken over all time origins  $t_0$ .  $\sigma_{\alpha\beta}$  is the stress tensor of the system [25]

$$\sigma_{\alpha\beta} = m \sum_{i=1}^N v_{i\alpha} v_{i\beta} + \frac{1}{2} \sum_{i \neq j}^N r_{ij\beta} F_{ij\alpha}, \quad (8)$$

where  $m$  is the monomer mass,  $v_{i\alpha}$  is the  $\alpha$ -component of the velocity of atom  $i$ ,  $r_{ij\beta}$  is the  $\beta$ -component of the vector  $\mathbf{r}_{ij}$  separating monomers  $i$  and  $j$ , and  $F_{ij\alpha}$  is the  $\alpha$ -component of the force exerted on monomer  $i$  by monomer  $j$ . The sum runs over all  $N$  monomers. For the calculation of  $G(t)$  we employ a fast Fourier transform [21], which accelerates the calculation by several orders of magnitude compared to the direct calculation method.

Figure 10 shows  $\eta$  as a function of  $J$ . Above the percolation threshold ( $J \lesssim 1.15$ ), the viscosity increases gradually with decreasing temperature. However, in accordance with the behavior of the diffusion coefficient,  $\eta$  starts to increase rapidly at the onset of percolation and micelle formation, and is described by an Arrhenius law.

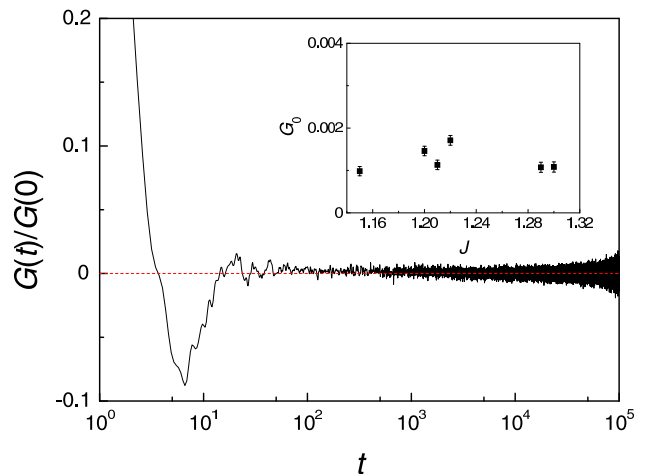


FIG. 11: Normalized stress autocorrelation function  $G(t)$  for  $J = 1.22$ . The plateau value  $G_0$  is small but distinctly nonzero, as shown in the inset. In addition, the plateau value does not exhibit a clear temperature dependence.

Experimentally, gelation is characterized by the appearance of a plateau in the stress autocorrelation function  $G(t)$ . In our simulations, we observe such a plateau for all temperatures below the percolation threshold. The plateau extends to longer times upon decreasing temperature, but eventually  $G(t)$  decays to zero. Since we use the “atomistic” (i.e., monomer-based) representation of the stress tensor  $\sigma_{\alpha\beta}$  in Eq. (7), the results exhibit relatively large fluctuations. Figure 11 shows a representative example. The plateau value  $G_0$  is small, but clearly nonzero, as shown in the inset.  $G_0$  is found to be only weakly dependent on temperature, and no clear trend can be identified, implying that the rapid increase in  $\eta$  (Fig. 10) arises from an increase in relaxation time rather than from a variation in  $G_0$ . The integration (6) partially suppresses the statistical fluctuations present in  $G(t)$ , but the uncertainties in  $\eta$  still reflect the computational challenges, in particular at low temperatures. While the strong increase in viscosity follows unambiguously from Fig. 10, we emphasize that the largest relaxation times (to be discussed below) are still much smaller than the experimentally observed relaxation times for physical gels, which range from microseconds to seconds [1]. Thus, only for (computationally inaccessible) temperatures far below the percolation threshold would the system investigated here undergo a sol-gel transition.

Following Ref. [11], we employ the non-Gaussian parameter  $\alpha_2$  for the single-chain center-of-mass displacement [26],

$$\alpha_2 \equiv \frac{3}{5} \frac{\langle r(t)^4 \rangle}{\langle r(t)^2 \rangle^2} - 1, \quad (9)$$

to estimate a characteristic time. This parameter equals zero for both the ballistic and the diffusive regime. As shown in Fig. 12,  $\alpha_2$  increasingly deviates from zero as the temperature is decreased, reflecting the heterogeneous dynamics resulting from the hopping of endblocks

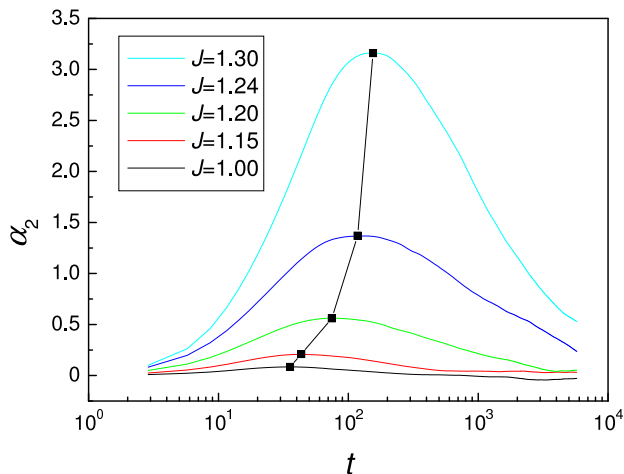


FIG. 12: The non-Gaussian parameter  $\alpha_2$  as a function of time at different inverse temperatures  $J$ . The deviation of  $\alpha_2$  from zero is indicative of the heterogeneous dynamics caused by the hopping of endblocks between bundles. The peak positions (squares) are used to define a characteristic time  $\tau$ .

between bundles. Also the maximum in  $\alpha_2$ , from which we extract a characteristic time  $\tau$ , shifts to larger times upon cooling. At short and long times,  $\alpha_2$  goes to zero, confirming the expected behavior for the ballistic and diffusive regimes, respectively. At intermediate times, however,  $\alpha_2$  deviates from zero and the deviation increases as the temperature is lowered. The positive deviation indicates the presence of anomalously fast chains, very similar to the heterogeneous dynamics observed in glass-forming liquids [27]. Figure 13 displays  $\tau$  as a function of  $J$ , on a log-linear scale. We see that the values of  $\tau$ , which extend up to approximately  $500\tau_0$  for the lowest temperatures, also follow an Arrhenius law, with a similar change in slope as observed for the diffusion coefficient and the viscosity. The mean-square displacement corresponding to  $\tau$  (cf. Fig. 8) is much smaller than the typical “hopping distance” or bundle separation (cf. Fig. 7), comparable to what is observed for glassy systems. Likewise, the observed values of  $\tau$  are much smaller than the relaxation times that follow from the extent of the plateau in  $G(t)$ , which are approximately given by  $\eta/G_0(J)$ .

Finally, we demonstrate the similarity of our dilute polymer solution to a glass-forming liquid by considering how well the Stokes–Einstein relation is obeyed. For a Newtonian fluid, we expect the product of the diffusion coefficient and the viscosity to obey  $D\eta = k_B T / 4\pi R_h$ , where  $R_h$  is the hydrodynamic radius. The product of  $D$  and  $\eta$  is plotted as a function of  $J$  in Fig. 14. The behavior of the end-to-end distance (Fig. 6) suggests that  $R_h$  will change only weakly with temperature, and even may increase as the temperature is lowered. In combination with the linear temperature dependence of the numerator of the Stokes–Einstein relation (i.e., inverse dependence on  $J$ ), the steep *increase* in  $D\eta$  for  $J \gtrsim J^*$  indicates a clear breakdown of this relation once micel-

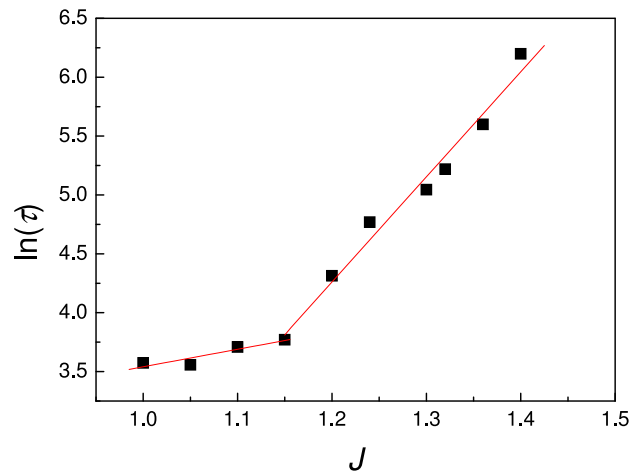


FIG. 13: The characteristic time  $\tau$  as extracted from Fig. 12, as a function of inverse temperature  $J$  on a log-linear scale. Two relaxation regimes can be discerned, separated by the percolation threshold  $J^* \approx 1.15$ .

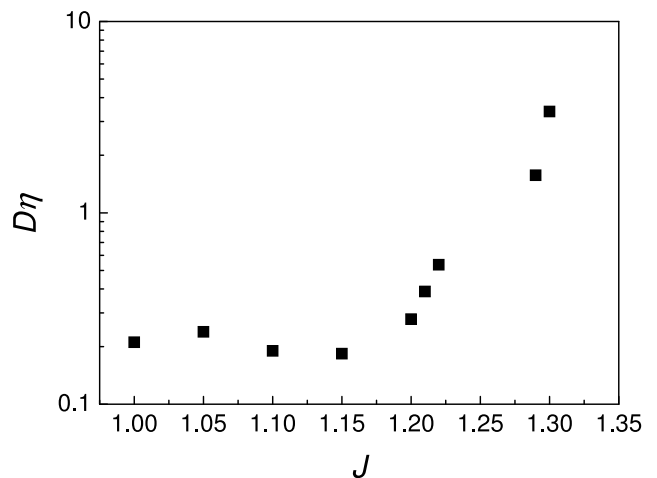


FIG. 14: The product  $D\eta$  as a function of  $J$ . Below  $J^* = 1.15$ ,  $D\eta$  varies weakly, consistent with the prediction of the Stokes–Einstein equation. Above  $J^*$ , an order of magnitude increase of  $D\eta$  within a narrow temperature windows clearly deviates from the Stokes–Einstein equation.

lization and network formation set in. The diffusion coefficient is *larger* than would be predicted on the basis of the viscosity shown in Fig. 10. The precise microscopic origin of this behavior, however, remains to be determined. As shown in the inset of Fig. 11, this breakdown does *not* result from a temperature dependence in the modulus  $G_0$ .

#### IV. CONCLUSION

We have studied the structural and dynamical properties of a solution of associative A-B-A triblock copolymers. The semiflexible character of the center (B) blocks, in combination with the attraction between endgroups,



allows these polymers to form a gel at remarkably low concentrations. The molecular dynamics simulations presented here form a natural extension of earlier work on semiflexible chains [17], which however only addressed structural properties. In addition, we observe dynamic effects that bear close resemblance to those reported in Ref. [11] for a lattice-based model studied by Monte Carlo simulations and to those reported in Ref. [15] for micelle formation. However, the solutions in either of these studies had a significantly higher polymer concentration. Furthermore, the micelle solution was found to exhibit geometric percolation at all temperatures and the dynamic changes were linked to the thermodynamic micelle transition. We observe that all dynamic changes are correlated with micellization and the simultaneous emergence of a percolating network of polymer chains, in which bundles of rigid endblocks act as network junctions. Upon a further decrease in temperature, the hydrophobic blocks tend to align within a bundle, forming a microcrystalline-like structure. The resulting strong binding of the chains is responsible for the mechanical stability of the gel-like network. On a larger scale, the bundles distribute more regularly at lower temperature, as indicated by the appearance of peak at the average bundle separation in the hydrophobe–hydrophobe radial distribution function.

The change in the dynamical behavior of the solution that occurs upon micellization and network formation is reflected in the diffusion constant, the viscosity and the maximum in the non-Gaussian parameter. The temperature dependence of all these properties changes near the percolation threshold and is well described by an Arrhenius law, similar to what is observed for strong glass formers. The activation barrier in our system has

a clear *thermodynamic* origin, namely the strong attraction between endblocks that are part of the same microdomain or “bundle.” Thus, there are similarities with the diffusion of diblock copolymers in a lamellar phase, which also exhibits an exponential decay with temperature [28, 29, 30]. Recently, this type of dynamics has attracted attention in the context of slow dynamics in systems with frustration-limited domains (see Ref. [31] and references therein).

Finally, we note that, while we observe a finite plateau in the stress autocorrelation function, as would be expected for a gel-forming material, the dynamics in our systems are still faster than in actual experimental gels. Thus, the sol–gel transition only occurs at a temperature far below the percolation threshold.

### Acknowledgments

Helpful comments by Ken Schweizer are gratefully acknowledged. This work is supported by the American Chemical Society Petroleum Research Fund under Grant No. 38543-G7 and by the National Science Foundation through an ITR grant (DMR-03-25939) via the Materials Computation Center at the University of Illinois at Urbana-Champaign. Access to computational facilities at Oak Ridge National Laboratory (via Grant No. CNMS2003-005 at the Center for Nanophase Materials Sciences) was supported by the U.S. Department of Energy, under contract DE-AC05-00OR22725 with UT-Battelle, LLC.

- 
- [1] Rubinstein, M.; Dobrynin, A. V. *Curr. Opin. Colloid Interface Sci.* 1999, 4, 83.
  - [2] Tanaka, F.; Matsuyama, A. *Phys. Rev. Lett.* 1989, 62, 2759.
  - [3] Tanaka, F. *Macromolecules* 1989, 22, 1988.
  - [4] Stockmayer, W. H. *Macromolecules* 1991, 24, 6367.
  - [5] Tanaka, F.; Stockmayer, W. H. *Macromolecules* 1994, 27, 3943.
  - [6] Semenov, A. N.; Rubinstein, M. *Macromolecules* 1998, 31, 1373.
  - [7] Groot, R. D.; Agterof, W. G. M. *J. Chem. Phys.* 1994, 100, 1649.
  - [8] Groot, R. D.; Agterof, W. G. M. *J. Chem. Phys.* 1994, 100, 1657.
  - [9] Groot, R. D.; Agterof, W. G. M. *Macromolecules* 1995, 28, 6284.
  - [10] Kumar, S. K.; Panagiotopoulos, A. Z. *Phys. Rev. Lett.* 1999, 82, 5060.
  - [11] Kumar, S. K.; Douglas, J. F. *Phys. Rev. Lett.* 2001, 87, 188301.
  - [12] Larson, R. G. *The structure and rheology of complex fluids*; Oxford U.P.: Oxford, 1998.
  - [13] Semenov, A. N.; Joanny, J.-F.; Khokhlov, A. R. *Macromolecules* 1995, 28, 1066.
  - [14] Khalatur, P. G.; Khokhlov, A. R. *Macromol. Theory Simul.* 1996, 5, 877.
  - [15] Bedrov, D.; Smith, G. D.; Douglas, J. F. *Europhys. Lett.* 2002, 59, 384.
  - [16] Tanaka, F.; Edwards, S. F. *J. Non-Newton. Fluid Mech.* 1992, 43, 247.
  - [17] Khalatur, P. G.; Khokhlov, A. R.; Kovalenko, J. N.; Mologin, D. A. *J. Chem. Phys.* 1999, 110, 6039.
  - [18] Petka, W. A.; Harden, J. L.; McGrath, K. P.; Wirtz, D.; Tirrell, D. A. *Science* 1998, 281, 389.
  - [19] Smith, W.; Forester, T. J. *Molec. Graphics* 1996, 14, 136.
  - [20] Frenkel, D.; Smit, B. *Understanding Molecular Simulation*, 2nd ed.; Academic: San Diego, 2002.
  - [21] Allen, M. P.; Tildesley, D. J. *Computer Simulation of Liquids*; Clarendon: Oxford, 1987.
  - [22] Blöte, H. W.; Luijten, E.; Heringa, J. R. *J. Phys. A* 1995, 28, 6289.
  - [23] Rubinstein, M.; Colby, R. H. *Polymer Physics*; Oxford University Press: Oxford, 2003.
  - [24] Kob, W. *J. Phys.: Condens. Matter* 1999, 11, R85.
  - [25] Haile, J. M. *Molecular Dynamics Simulation: Elementary Methods*; Wiley: New York, 1992.

- [26] Rahman, A. Phys. Rev. 1964, 136, A405.
- [27] Kob, W.; Donati, C.; Plimpton, S. J.; Poole, P. H.; Glotzer, S. C. Phys. Rev. Lett. 1997, 79, 2827.
- [28] Barrat, J.-L.; Fredrickson, G. H. Macromolecules 1991, 24, 6378.
- [29] Lodge, T. P.; Dalvi, M. C. Phys. Rev. Lett. 1995, 75, 657.
- [30] Guenza, M.; Tang, H.; Schweizer, K. S. Macromolecules 1997, 30, 3423.
- [31] Geissler, P. L.; Reichman, D. R. Phys. Rev. E 2004, 69, 021501.